Flowfield Produced by Rocket Exhaust Impingement of a Multitube Launcher

Stanley A. Bouslog,* John J. Bertin,† and William B. Wingert II*
The University of Texas at Austin, Austin, Texas

When a rocket is launched from a multitube launcher, its exhaust gases impinge on the launcher assembly, creating a complex viscous/shock interaction flowfield. An experimental program has been conducted in which simulated underexpanded exhaust plumes impinged on the face of a multi-tube launcher. The test variables included: distance from the nozzle-exit plane to the launcher assembly, stagnation pressure of the simulated rocket, and number of open tubes. Supercritical flows were obtained in which a large fraction of the exhaust gas spread over the face of the launcher assembly with attendant high pressures. The most important parameter in defining the impingement flowfield was the ratio of plume diameter/tube diameter.

Nomenclature

d = diameter
h = distance between nozzle-exit plane and face of the launcher
h_1^* = distance h at which strong instability occurs
h_2^* = distance h at which weak instability occurs
M = Mach number
p = pressure
r = radius
x,y,z = coordinates of right-handed coordinate system
γ = ratio of specific heats
θ_{ne} = nozzle-exit angle

Superscript

$( )^*$ = sonic conditions

Subscripts

atm = atmospheric conditions
max = maximum value
ne = nozzle-exit conditions
t = tube
tl = stagnation conditions

Introduction

THE complex viscid/inviscid interaction flowfield created by the impingement of a supersonic jet on a nearby surface occurs in a variety of applications. For some applications, the axis of the jet is parallel to the surface,[1,2] such as might occur when a missile is launched from an airplane or during stage separation. The subject of the present study is the flowfield that occurs when a rocket exhaust impinges on the surface of a multitube launcher assembly. In the study of the jet-impingement flowfield for launchers, most investigators have simulated the impingement of a supersonic jet onto a flat, solid surface that is perpendicular to the jet axis. Gummer and Hunt[3] found that the impingement of a properly expanded, uniform jet that was located approximately $1r_{ne}$ above a plate produced a static pressure distribution that was a maximum at the centerline and decreased slowly in the radial direction. The main features of the flow for these conditions included a symmetric shock wave spanning the jet that was convex upward causing an outward deflection of the streamlines and the reduction of the flow velocities downstream of the shock wave to subsonic speeds.

In an experimental investigation of a supersonic jet impinging onto a circular disk, whose diameter was four times that of the jet, Henderson[4] observed a sudden and intense increase in the noise level generated by the interaction. The increase occurred when the exit-plane Mach number was approximately 2 and the plate was $4\text{-}7r_{ne}$ from the exit plane.

As the distance h from the nozzle-exit plane to the barrier is increased, it is apparent that the shock structure changes. Based on the investigations of Semiletenko and Uskov,[5] Ginzburg et al.,[6] and Golubkov et al.,[7] the variation of the wave structure in the interaction flowfield of the impinging jet with distance is as follows.

1) When h is relatively small, the central compression shock wave is convex toward the nozzle. This is consistent with the structure observed by Gummer and Hunt.[3]

2) As h is increased, the central compression shock wave may pass through inflections becoming concave toward the nozzle.

For cases 1) and 2), Ginzburg et al.[6] note that the static pressure distribution has a maximum at the center of the barrier.

3) When the distance between the nozzle-exit plane and the plate is increased further, the pressure at the centerline decreases more rapidly than that near the edge. Semiletenko and Uskov[5] note that the wave structure at a critical value of h (which will be designated h_1^* for this report) fluctuates at a high frequency. This unstable interaction is accompanied by the generation of strong acoustic waves. Ginzburg et al.[6] note that the strong instability and the sonic vibration develop when the pressure at the center of the obstruction becomes equal to that in the peripheral region.

4) Ginzburg et al.[6] noted further that, when h was increased above h_1^*, there was a further reduction of the pressure in the central region, while the pressure at the periphery remained about the same. Thus, for $h > h_1^*$, the character of the static pressure distribution on the obstacle changed, exhibiting a peak near the periphery of the impinging jet.

Submitted June 7, 1982; presented as Paper 82-0946 at the AIAA/ASME 3rd Joint Thermophysics, Fluids, Plasma and Heat Transfer Conference, St. Louis, Mo., June 7-11, 1982; revision received Aug. 16, 1983. This paper is declared a work of the U.S. Government and therefore is in the public domain.

*Research Assistant, Department of Aerospace Engineering and Engineering Mechanics. Member AIAA.

†Bettie Margaret Smith Professor of Engineering, Department of Aerospace Engineering and Engineering Mechanics. Associate Fellow AIAA.

For values of $h > h_1^*$, the shock structure exhibits the elements shown in Fig. 1. There is a central compression shock wave (CSW) that is concave toward the nozzle. An oblique, reflected shock wave (RSW) occurs outboard of the intersection of the CSW and the lip shock wave (LSW). Because the reflected shock wave is more oblique and relatively weaker than the central compression shock wave, the total pressure is greater downstream of the RSW than downstream of the CSW. Thus, as the flow decelerates toward the plate, a peak occurs in the local pressure near the periphery of the impinging jet.

Using schlieren photographs, oil-flow patterns, and hot-wire probes, Ginzburg et al.[6] recorded the existence of a central region of flow reversal. The dividing streamline on the plate occurred in the region of the peripheral pressure peak. Pressure distributions for $h < h_1^*$ and for $h > h_1^*$, as taken from Ref. 6, are reproduced in Fig. 2. Belov et al.[8] have used integral equations and an approximate flow model similar to that of Fig. 1 in order to estimate the heating to the surface of the plate.

5) As h is increased still further, a second weak, instability is observed.[5,6] The acoustic field and the fluctuations in the wave structure at this value of h (which will be designated h_2^*) are much weaker than those observed during the first instability mode.

6) The weak instability is followed by a stepwise transition to a stable mode. In this case, the shock wave structure corresponds to the wave structure of a free-jet exhausting into the ambient atmosphere, but there is a second, centered shock wave that is produced as the flow encounters the plate. This second CSW is initially convex to the nozzle and then, as h is increased, becomes concave to the nozzle.

7) As the nozzle-exit plane moves far from the obstruction, viscous effects spread across the entire jet. The pressure distribution on the plate then becomes relatively constant across the impingement (see Ref. 9).

The values of h_1^* and of h_2^* at which the interaction flowfield changes character depend on the conditions in the nozzle-exit plane, on the ratio of specific heats of the exhaust gas γ, on the jet-expansion ratio (p_{ne}/p_{atm}), and on the relative dimensions of the jet and the obstruction.

In all the investigations discussed thus far, the jet exhaust impinged on a solid obstruction. However, for a rocket exiting from a launcher, the obstruction contains one or more openings through which the exhaust gases can pass. The present report discusses data that were obtained at the Rocket Exhaust Effects Facility at the University of Texas at Austin in which a simulated underexpanded rocket-exhaust-plume impinged on the face of a multitube launcher. The viscid-inviscid shock interaction flowfield was defined using pressure measurements and flow visualization photographs.

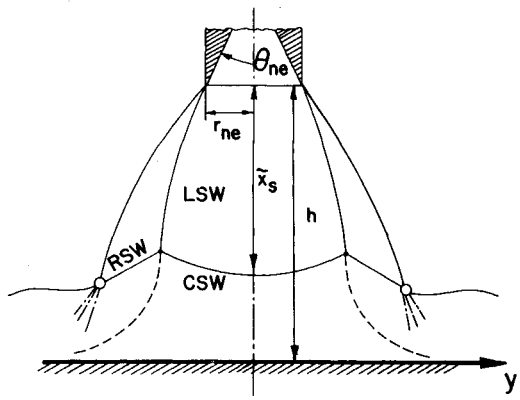

Fig. 1 Shock-wave structure of an underexpanded jet impinging on a flat plate.[6]

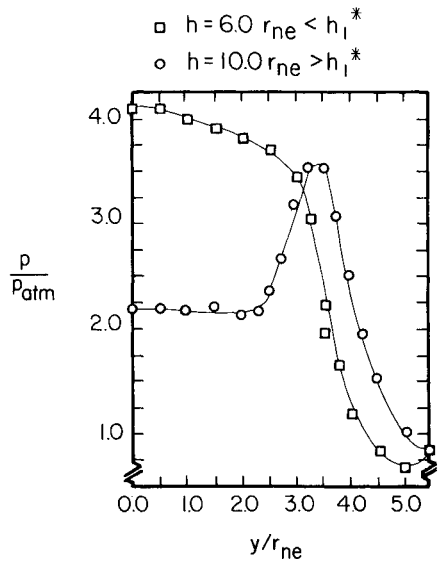

Fig. 2 Static pressure distribution on a flat plate at $M_{ne} = 2.0$, $\theta_{ne} = 10$ deg and $p_{ne} = 5.1\, p_{atm}$.[6]

Experimental Program

Simulated rocket exhaust plumes were obtained by accelerating unheated, compressed air (the test gas) through a pipe with a convergent-divergent nozzle (the simulated rocket). The simulated rocket (i.e., the pipe/nozzle configuration) was threaded to a high-pressure supply line and held firmly in place by a yoke assembly. The model of the multitube launcher was mounted on a carriage assembly that allowed translation in the x (or streamwise), y, and z directions, and rotation in the pitch and yaw planes. An isometric sketch of the basic rocket/launcher configuration is presented in Fig. 3.

Simulated Rocket

A sketch illustrating the geometry of the 10 deg conical convergent/divergent nozzle used to produce the simulated rocket exhaust is presented in Fig. 4. The nozzle-exit radius, r_{ne}, which is used as the characteristic dimension to nondimensionalize the length parameters, is 1.453 cm (0.572 in.). The area ratio of the nozzle, A_{ne}/A^*, is 2.242. If one assumes isentropic gas flow relations, the nozzle-exit plane Mach number is 2.32. However, because of the relatively sharp throat, shock waves originated near the throat, as will be evident in the shadowgraphs of the exhaust flow. A total of 32 diametrically opposed static-pressure orifices were located in

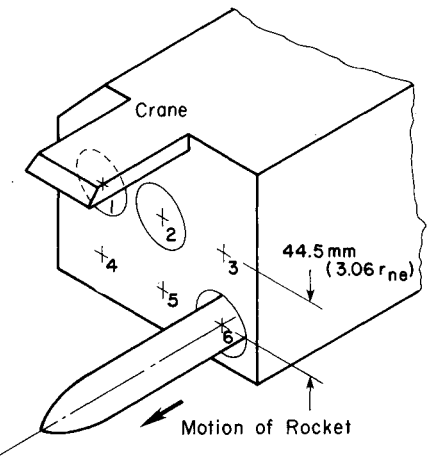

Fig. 3 An isometric sketch of the simulated rocket/multitube launcher configuration.

the outer surface of the simulated rocket, which permitted the direct measurement of pressures on its outer surface.

Simulated Launcher

A model of one half of a multitube launcher assembly containing 12 tubes has been constructed. As shown in Fig. 3, only three tubes were simulated in the model. The other three tubes remained "covered" for these tests. The relative position of tubes 1, 2, and 6 and of the overhang which simulates a telescoping crane used to reload the launcher are illustrated in Fig. 3. The internal radius of the constant cross-sectional area launch tubes was $1.44r_{ne}$. The front face of the simulated launcher was fitted with 81 static pressure orifices, each 0.064 cm (0.025 in.) in diameter.

Test Program

Three rocket/launcher configurations were simulated in this experimental program: rocket launching out of 1) tube 1; 2) tube 2; or 3) tube 6. While "launching" the simulated rocket out of one tube, the remaining tubes could be left covered or be opened, as if a rocket had already been launched from that tube in a simulated ripple firing. Before each run, the rocket was aligned so that its axis was colinear with that of the launch tube of interest. It should be noted that despite the painstaking alignment procedure, exhaust-pressure loading on the launcher introduced a small misalignment between the rocket and the launcher during the run.

During the test, the stagnation pressure in the nozzle reservoir and, therefore, the mass-flow of the unheated air were controlled by the test operator. Once steady-state conditions were obtained at the desired chamber pressure, data were then recorded. Data were taken for nozzle-exit plane positions of 2.0, 4.0, 6.0, 8.0, 10.0, 12.0, and $15.0r_{ne}$ from the front of the launcher, and for chamber pressures of 7.58×10^6, 4.83×10^6, and 2.76×10^6N/m^2 (1100, 700, and 400 psi).

In addition to pressure data, photographic data were also obtained during this test program. Besides providing an illustration of the general features of the flowfield, the shadowgraphs of exhaust impingement allowed the measurement of shock positions. For additional information about the models, the tests, or the measurements, and additional data not presented in the present paper, the reader is referred to Ref. 10.

Discussion of Results

As discussed in the Introduction, one can identify distinctively different flowfields that result when an exhaust plume impinges on a plate. The type of impingement flowfield that exists depends on the diameter of the exhaust plume, the size of the plate, and the distance from the nozzle-exit plane to the plate. Many of the flow characteristics observed in the investigations of the impingement flowfields for plates and disks also were observed in the present investigation, where there was a large opening in the plate. However, because of the presence of a hole in the plate, an important characteristic dimension was found to be the diameter of the plume relative to the diameter of the tube.

Characterization of the Impingement Flowfield

Shadowgraphs of the exhaust plume as a free jet are presented in Fig. 5 for three stagnation pressures: 2.76×10^6, 4.83×10^6, and 7.69×10^6N/m^2. Included in the photographs are scales depicting the nondimensional axial coordinate and the internal diameter of the launch tube. In the subsequent discussion, the relation of these characteristic dimensions to the impingement flowfield will be discussed. These photographs are used to provide insights into the relation between the characteristic parameters and the impingement flowfield.

When the stagnation pressure is relatively low, the boundary of the free-jet plume does not intersect the cylinder representing the launch-tube wall. Such is the case when $p_{tl}=2.76\times10^6$ N/m^2, as shown in Fig. 5a. At intermediate pressures, e.g., $p_{tl}=4.83\times10^6$ N/m^2, the free-jet plume is slightly larger than the internal diameter of the launch tube, Fig. 5b. At the highest stagnation pressures of the present program, a large portion of the free-jet plume lies outside the boundary of the launch tube, e.g., Fig. 5c for $p_{tl}=7.69\times10^6$ N/m^2.

For purposes of this report, there were two characteristic impingement flowfields: 1) subcritical, i.e., one in which almost all of the exhaust flow is swallowed by the open launch tube, and 2) supercritical, i.e., one in which a strong shock-wave system is formed and a large fraction of the exhaust flow spreads over the face of the launcher. The supercritical flow occurs when the stagnation pressure and the distance from the nozzle-exit plane to the launcher surface are such that a strong shock wave is produced when the exhaust impinges on the rim of the tube. Because of the large decrease in stagnation pressure across the normal shock wave, the area of the launch tube is not large enough to pass all of the exhaust gases and the flow in the launch tube is "choked." As a result, a large fraction of the exhaust gases flow radially across the face of the launcher and the remainder continues down the tube. As will be discussed, the impingement flowfields over the face of the launcher assembly when the flow is supercritical and when $h>h_l^*$ are similar to those described as type

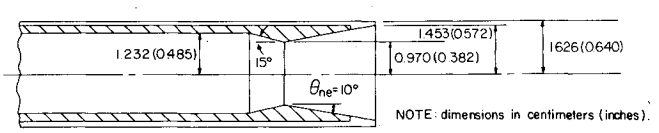

Fig. 4 Sketch of conical convergent/divergent nozzle simulating rocket.

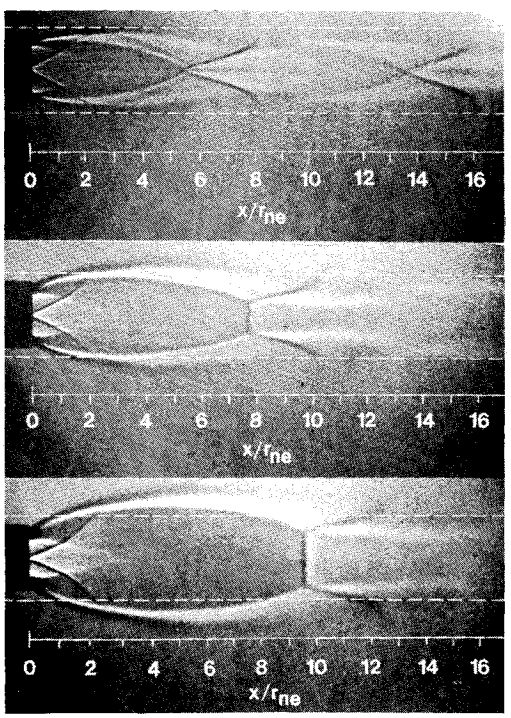

Fig. 5 Shadowgraphs of the exhaust plume as a free jet.

4 for the solid plates, as discussed in the Introduction and illustrated in Figs. 1 and 2.

The characteristic features of a subcritical flow and of a supercritical flow are illustrated in the composite figures of Fig. 6, in which a shadowgraph of the impinging exhaust has been superimposed on a graph of the experimentally determined isobars for the face of the launcher assembly. The surface pressures are given in atmospheres. The flowfield depicted in Fig. 6a is for a separation distance h of $10r_{ne}$ with the reservoir pressure p_{tl} equal to 4.86×10^6 N/m^2. That presented in Fig. 6b was obtained at the same separation distance, i.e., $h=10r_{ne}$, but with the reservoir pressure equal to 7.52×10^6 N/m^2.

Although the flow is subcritical for $p_{tl}=4.86\times10^6$ N/m^2, the impinging exhaust produces high surface pressures near the rim of the open tube. The surface pressure decreases with radial distance. As noted earlier, the movement of the launcher due to the pressure load produces an asymmetric pressure distribution. At the higher stagnation pressure, i.e., $p_{tl}=7.52\times10^6$ N/m^2, there is an "island" of high pressure near the periphery. Thus, the pressure distribution is similar to that observed by the Soviet researchers, as shown in Fig. 2 for the case where $h>h_j^*$.

Since the ratio of the plume diameter to the launch-tube diameter is a function of the stagnation pressure and of the separation distance between the nozzle-exit plane and the launcher, these two parameters can be used to characterize the impingement flowfield. They are used in the following discussion to correlate the onset of transition from subcritical flow to supercritical flow. To those actually present when the tests were conducted, the most apparent indication of the transition from subcritical flow to supercritical flow was a dramatic change in the sound emitted by the impinging plume. Other, albeit less graphic, means (such as shock structure and pressure fields) also could be used to define the transition.

The transition values of the stagnation pressure are presented as a function of the nozzle-exit position, h/r_{ne}, in Fig. 7. The open symbols represent minimum stagnation pressure required to obtain supercritical flow. They were recorded as the chamber pressure was increased slowly. Once supercritical flow had been established, it could be maintained at lower stagnation pressures than those required to initiate it. This phenomenon is indicated by the filled symbols, which represent the critical transition values of the stagnation pressure that were recorded as the chamber pressure was decreased. The filled symbols are consistently below the open symbols, indicating that once supercritical flow is established, it can exist at lower stagnation pressures than those required to initiate it. The difference becomes more pronounced as the distance between the nozzle-exit plane and the face of the launcher increases.

The flowfield changes that occur due to the exhaust impingement on the face of the launcher are illustrated in the pressure distributions and in the shadowgraphs presented in Figs. 8-11. The regions where the pressure exceeds 4 atm are highlighted by shading. These data represent the interaction that occurs when the nozzle-exit plane is $10r_{ne}$ from tube 2. Based on the data presented in Fig. 7, the threshold value of the nozzle stagnation pressure for obtaining supercritical flow when $h=10r_{ne}$ ranges from 4.70 to 4.95×10^6 N/m^2. When p_{tl} is below the threshold value most of the exhaust flow is swallowed by the open tube. As a result, the impinging exhaust plume is only slightly affected by the presence of the launcher, e.g., Figs. 8 and 9. The surface pressures are relatively high near the rim of the tube, decreasing with radial distance from the opening. For these subcritical flows, the maximum value of the surface pressure decreased as the stagnation pressure decreased. At the lowest stagnation pressure tested, i.e., $p_{tl}\approx2.76\times10^6$ N/m^2, the plume is of the same size as the tube diameter. Thus any effect of the exhaust plume on the pressure distribution is limited to the region near the edge of the open tube. The maximum surface pressure was less than 2 atm. Subatmospheric pressures were recorded at many of the orifices, as indicated by the broken isobars.

For those runs in which the stagnation pressure exceeds 5.0×10^6 N/m^2, there is a strong, central shock wave bounded by an oblique, reflected shock wave, e.g., Figs. 10 and 11. A large fraction of the exhaust gases flows over the face of the launcher assembly. "Annular rings" of high pressure occur near the periphery of the plume, downstream of the oblique, reflected shock wave. Thus, when the flow is supercritical ($h>h_j^*$), the interaction flowfield generated by a plume impinging on the face of the launcher assembly with a tube open is essentially the same as that which occurs when a plume impinges on a solid plate. The presence of the opening at these conditions apparently has only a secondary effect on the impingement interaction flowfield.

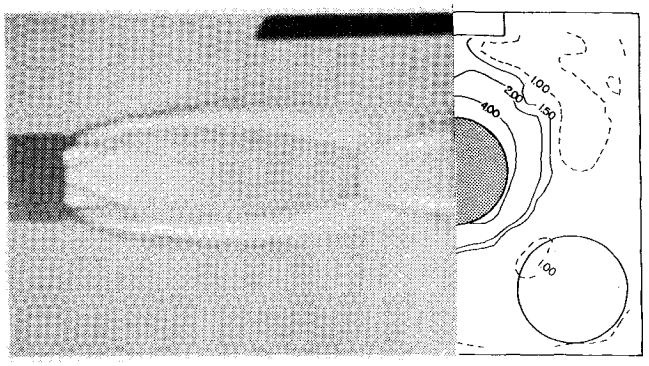

a) Subcritical flow, $p_{tl}=4.86\times10^6$ N/m^2 (705 psi).

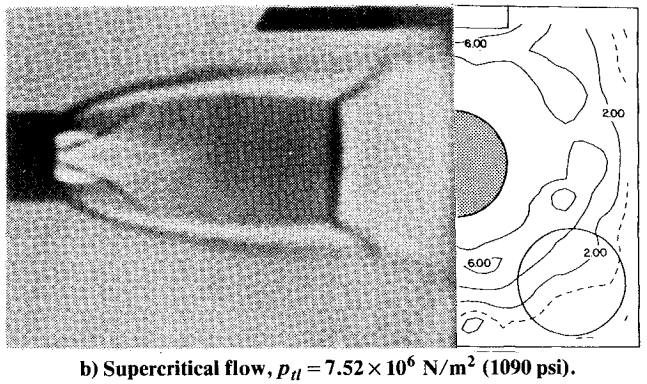

b) Supercritical flow, $p_{tl}=7.52\times10^6$ N/m^2 (1090 psi).

Fig. 6 Characteristics of subcritical and of supercritical flows ($h=10r_{ne}$). Pressure contours in atmospheres.

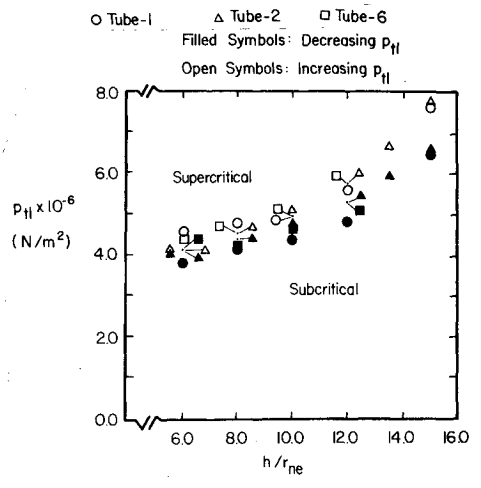

Fig. 7 The threshold values of the stagnation pressure.

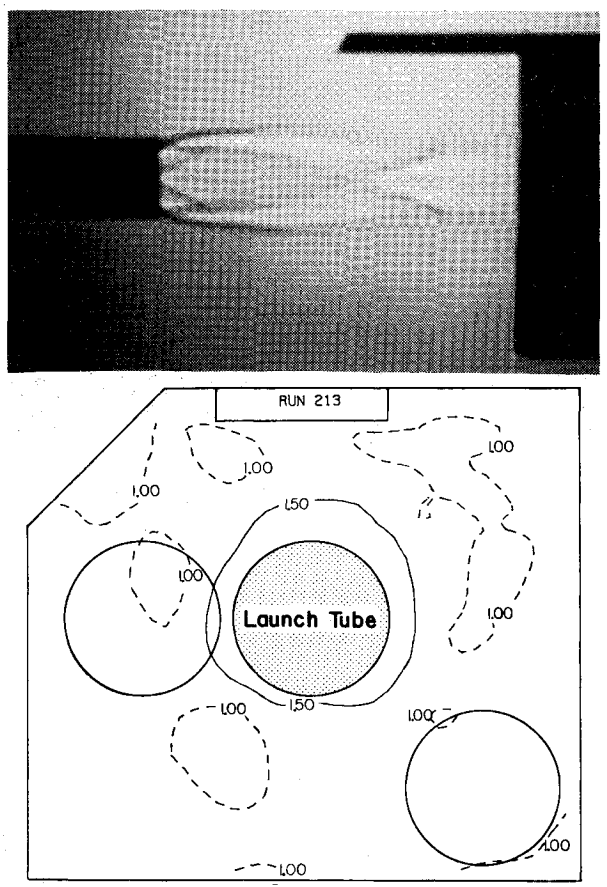

Fig. 8 Impingement flowfield, $h = 10r_{ne}$, $p_{tl} = 2.76 \times 10^6$ N/m^2.

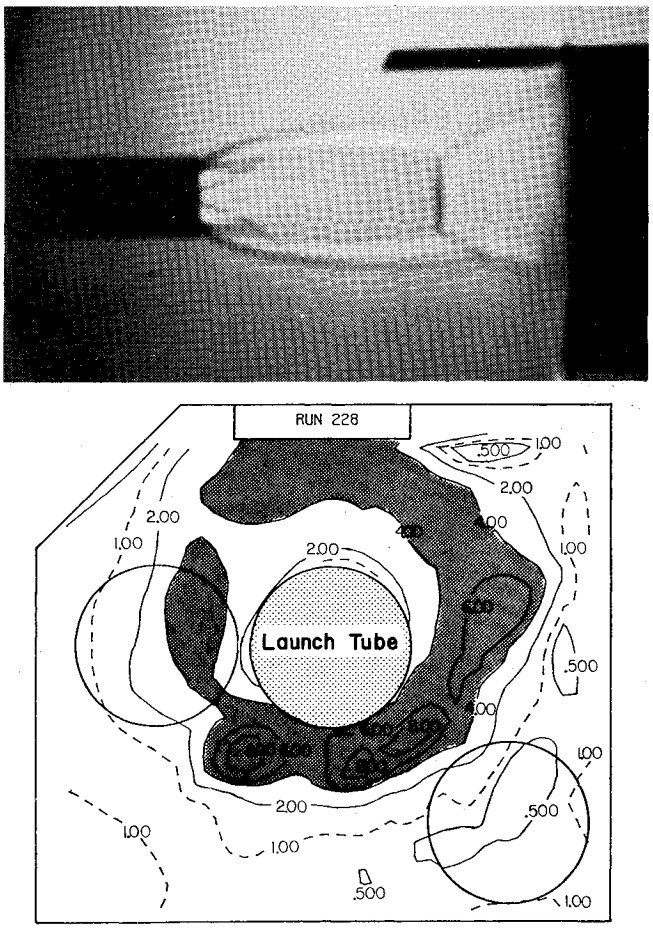

Fig. 10 Impingement flowfield, $h = 10r_{ne}$, $p_{tl} = 5.38 \times 10^6$ N/m^2.

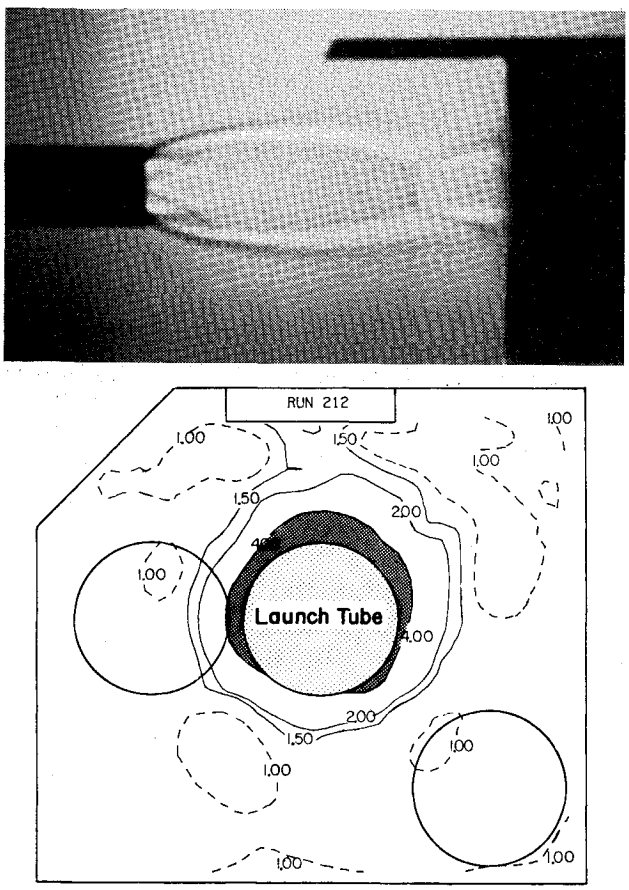

Fig. 9 Impingement flowfield, $h = 10r_{ne}$, $p_{tl} = 4.86 \times 10^6$ N/m^2.

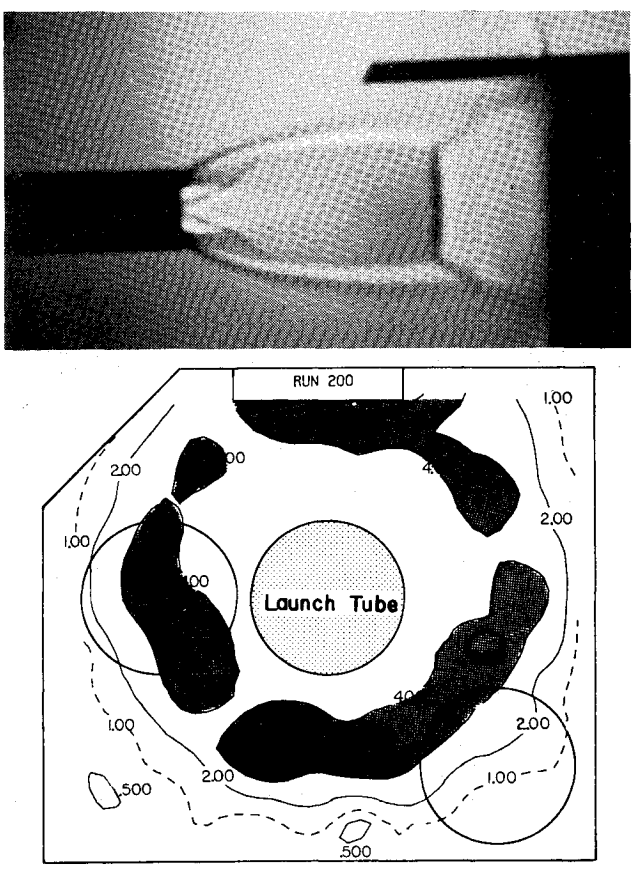

Fig. 11 Impingement flowfield, $h = 10r_{ne}$, $p_{tl} = 7.52 \times 10^6$ N/m^2.

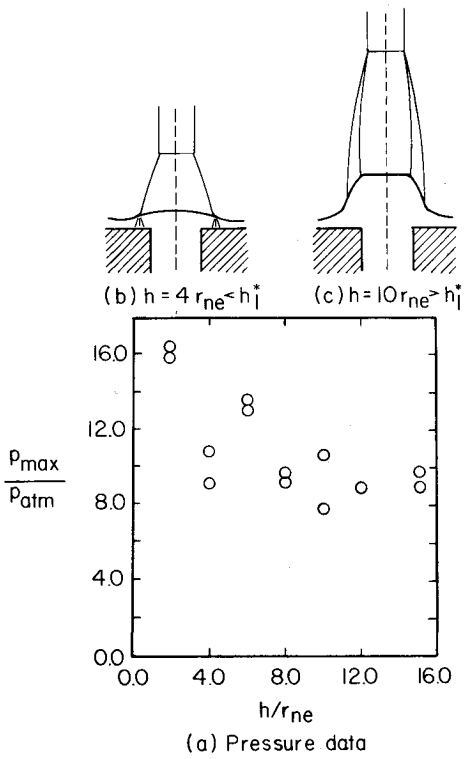

Fig. 12 The maximum pressures measured on the face of the launcher assembly, $p_{tl} \approx 7.58 \times 10^6$ N/m^2, tube 6.

The effect of the flowfield characteristics on the maximum pressures measured on the face of the launcher assembly is illustrated in the data presented in Fig. 12. The data for $p_{tl} \approx 7.58 \times 10^6$ N/m^2 are presented as a function of h/r_{ne} as the rocket was launched from tube 6. When the nozzle-exit plane is relatively near the surface, i.e., $h < h_l^*$, the viscid/inviscid interaction is dominated by the normal shock wave that spans the impinging plume, Fig. 12b. As a result, the pressure on the face of the launcher is equal to the pressure downstream of a normal shock wave and is relatively high. As h increases, i.e., as the rocket moves away from the launcher, but remains less than h_l^*, the pressure downstream of the normal shock wave decreases. However, when $h \approx h_l^*$, the viscid/inviscid interaction flowfield changes to that described in Fig. 1 and Fig. 12c. Oblique shock waves appear near the periphery of the impinging plume. Since the stagnation pressure drop across an oblique shock wave is less than that across a normal shock wave, there is an increase both in the magnitude and in the radial location of the maximum pressure when this change in the shock structure occurs.

Effect of an Open Adjacent Tube

In determining the firing sequence of a multitube launcher assembly, it is of interest to investigate the effect that an open tube, adjacent to the launch tube, could have on the impinging flowfield. The pressures measured when the nozzle-exit plane is $10r_{ne}$ from tube 2, but the adjacent tube (tube 1) is open, are presented in Fig. 13. In general, the opening of the adjacent tube had only a slight effect on the pressure distributions measured on the face of the launcher. The small changes in the isobars may be as much due to the fairing of the measured data as to actual significant changes in the flow field. Measureable changes were observed during some runs, as discussed in Ref. 10, but they were observed only for specific configurations and were not the general rule.

Pressure Differentials Acting on the Rocket

When the exhaust gases from a rocket that is exiting a given launch tube impinge on the face of the launcher assembly, a

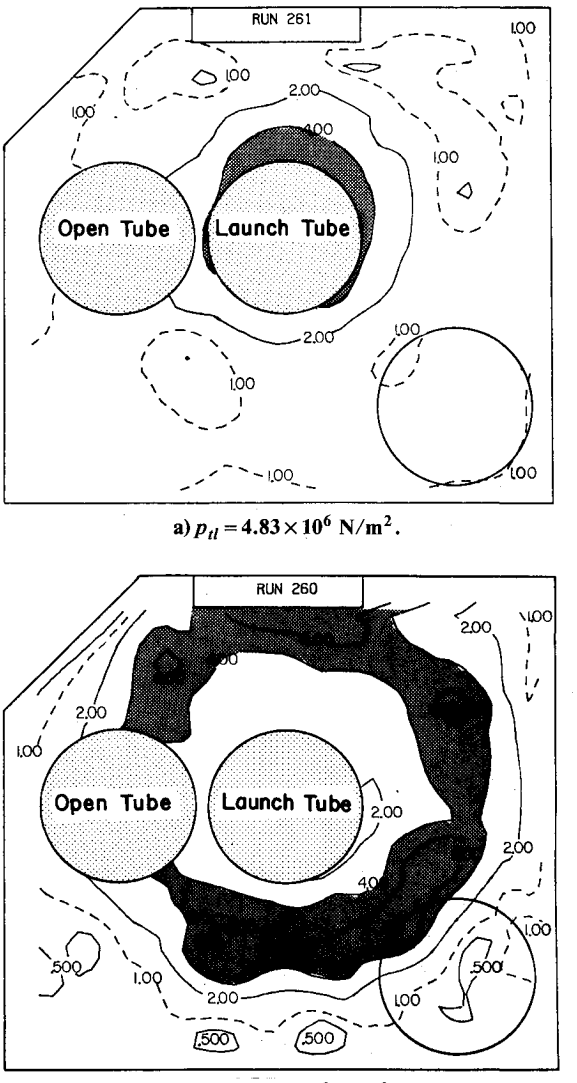

a) $p_{tl} = 4.83 \times 10^6$ N/m^2.

b) $p_{tl} = 7.52 \times 10^6$ N/m^2.

Fig. 13 The effect of adjacent open tubes 1 and 2, $h = 10r_{ne}$.

complex viscid/inviscid interaction occurs. As a result, a portion of the impinging flow can "splash-back" onto the rocket. The asymmetric character of this splash back flow can cause pressure differentials on the rocket. If large enough, the pressure differentials will affect the free-flight trajectory of the rocket.

As noted earlier, the external surface of the rocket model used in the present experimental program was instrumented with diametrically opposed orifices, allowing for the direct measurement of static pressures on its external surface. The maximum pressure differentials, i.e., the maximum value of the difference in the pressure measured at diametrically opposed orifices are presented in Fig. 14 for several launch conditions. Intuitively, one would expect the pressure differentials divided by the atmospheric pressure to be small when most of the exhaust gas is swallowed by the open tube. Furthermore, the effects of splash back would be expected to diminish as the nozzle-exit plane moves further from the face of the launcher. Thus, the maximum pressure differential would be expected to occur when the stagnation pressure is relatively high and when the nozzle-exit plane is near (but not immediately adjacent to) the face of the launcher. Data are presented for simulated launches from tubes 1, 2, and 6, both with a single tube open and with two tubes open, and for a stagnation pressure of approximately 7.58×10^6 N/m^2. The peak pressure differentials occur at a separation distance between 4.0 and $6.0r_{ne}$. Since the flowfield is supercritical for

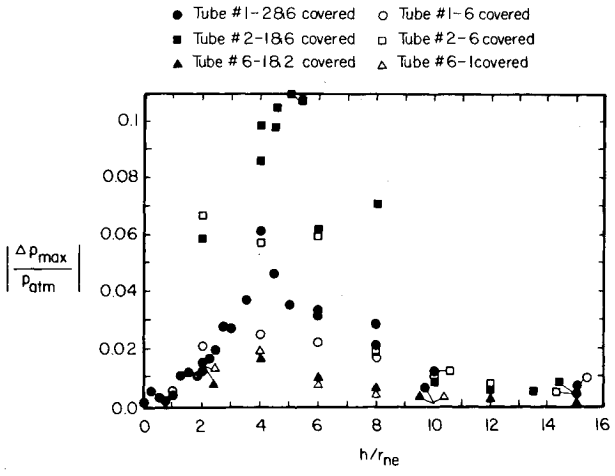

Fig. 14 The maximum pressure differential measured on the external surface of the rocket.

these conditions and the nozzle-exit plane is relatively close to the launcher, the data support the intuitive reasoning. The data indicate that the launcher geometry has an effect on the flow producing the pressure differentials. As might be expected, the pressure differentials are greatest when the rocket is launched from tube 2 and the exhaust flowfield is perturbed by the overhead crane directly above launch tube 2. Relatively large pressure differentials were measured for all separation distances less than $8.0r_{ne}$ for this launch configuration. For some launch conditions from tube 2, the largest static pressures acted on the top of the rocket. However, the angular location of the maximum static pressures measured on the rocket was not constant for all separation distances and all chamber pressures. In contrast, the maximum static pressures obtained for simulated launches for tubes 1 and 6 consistently acted on the outboard side of the rocket. The moment induced by these pressures could cause the rocker to veer away from the axis of the launch tube.

As noted earlier, the pressure differentials acting on the rocket were measured both with the adjacent tubes being covered and with the adjacent tubes open. The data of Fig. 14 indicate that generally the effect of splash-back on the rocket is less when the adjacent tube is open.

Concluding Remarks

An experimental program has been conducted in which simulated rocket exhaust plumes impinged on the face of a multitube launcher. For the range of variables considered in the present test program, the following conclusions are made.

1) An important characteristic dimension for the impingement flowfield is the ratio of the plume diameter to the diameter of the launch tube. For a given nozzle/launcher configuration, this ratio is a function of the stagnation pressure and of the separation distance between the nozzle-exit plane and the launcher.

2) When the stagnation pressure is relatively low, most of the exhaust gas is swallowed by the launch tube. High surface pressures are limited to the region near the rim of the launch tube.

3) Once a critical value of p_{t_l} is exceeded, the central shock wave increases in size and strength. For these supercritical flows, a large fraction of the exhaust gas flows across the face of the launcher, producing relatively high pressures over large areas of the surface of the launcher. When the flow is supercritical, the primary correlation parameter is the ratio h/h_l^*.

a) If $h<h_l^*$ the viscid/inviscid shock interaction structure is dominated by the central shock wave. The highest surface pressures occur near the rim of the launch tube.

b) When $h>h_l^*$, the central shock wave is bounded by an oblique, reflected shock wave and an annular ring of relatively high pressure occurs near the perphery of the impinging jet. The flowfield is similar to that observed when a supersonic jet impinges on a solid plate.

4) The maximum pressure differentials that act across the missile itself occur when the flow is supercritical and the nozzle-exit plane is near the face of the launcher. The largest pressure differentials were obtained, when the missile was launched from tube 2, which is in close proximity to the overhead crane structure. Although the pressure differentials were not as great in magnitude for launches from tube 1 or 6, the resulting pressure force consistently produced moments that would cause a missile launched from these tubes to veer away from the launch-tube axis.

Acknowledgment

This work was supported by the U.S. Army Missile Command through Contract DAAH01-81-C-B078.

References

[1]Vick, A. R. and Andrews, E. H. Jr., "An Experimental Investigation of Highly Underexpanded Free Jets Impinging Upon a Parallel Flat Surface," NASA TN-D-2236, June 1964.

[2]Ivanov, M. Y. and Nazarov, V. P., " 'Lateral' Interaction of a Supersonic Underexpanded Ideal-Gas Jet With Surfaces of Different Shape," *Izvestiya Akademii Nauk SSSR, Mekhanika Zhidkosti i Gaza,* No. 6, Nov.-Dec. 1974, pp. 3-8.

[3]Gummer, J. H. and Hunt, B. L., "The Impingement of a Uniform Axisymmetric, Supersonic Jet on a Perpendicular Flat Plate," *The Aeronautical Quarterly,* Vol. 22, Nov. 1971, pp. 403-420.

[4]Henderson, L. F., "Experiments on the Impingement of a Supersonic Jet on a Flat Plate," *Journal of Applied Mathematics and Physics,* Vol. 17, 1966, pp. 553-569.

[5]Semiletenko, B. G. and Uskov, V. N., "Empirical Formulas for Location Shock Waves in a Jet Impinging on a Barrier at Right Angles," *Inzhenerno-Fizicheskii Zhurnal,* Vol. 23, No. 3, Sept. 1972, pp. 453-458.

[6]Ginzburg, I. P., Semiletenko, B. G., and Uskov, V. N. "Experimental Study of Underexpanded Jets Impinging Normally on a Plane Baffle," *Fluid Mechanics-Soviet Research,* Vol. 4, No. 3, May-June 1975, pp. 93-105.

[7]Golubkov, A. G., Koz'menko, B. K., Ostapenko, V. A., and Solotchin, A. V., "On the Interaction of an Underexpanded Supersonic Jet with a Finite Flat Baffle," *Fluid Mechanics-Soviet Research,* Vol. 3, No. 1, Jan.-Feb. 1974, pp. 96-102.

[8]Belov, I. A., Ginzburg, I. P., and Shub, L. I., "Supersonic Underexpanded Jet Impingement upon Flat Plate," *International Journal of Heat and Mass Transfer,* Vol. 16, Nov. 1973, pp. 2067-2076.

[9]Pieski, E. T. and Roberts, D. J., "A Method to Define Low-Altitude Rocket Exhaust Characteristics and Impingement Effects," *Journal of Spacecraft and Rockets,* Vol. 7, April 1970, pp. 446-451.

[10]Bouslog, S. A., Bertin, J. J., and Wingert, W. B. II, "Impingement Flow-Fields for Tube-Launched Rockets," Fluid Dynamics Institute, The University of Texas at Austin, Tex., Rept. 82-101, May 1982.